DOI: 10.1002/anie.201405681

Microreactor Imaging

Lab-on-a-Chip Reactor Imaging with Unprecedented Chemical Resolution by Hadamard-Encoded Remote Detection NMR**

Ville-Veikko Telkki, Vladimir V. Zhivonitko, Anne Selent, Gianmario Scotti, Jarmo Leppäniemi, Sami Franssila, and Igor V. Koptyug*

Abstract: *The development of microfluidic processes requires information-rich detection methods. Here we introduce the concept of remote detection exchange NMR spectroscopy (RD-EXSY), and show that, along with indirect spatial information extracted from time-of-flight data, it provides unique information about the active regions, reaction pathways, and intermediate products in a lab-on-a-chip reactor. Furthermore, we demonstrate that direct spatial resolution can be added to RD-EXSY efficiently by applying the principles of Hadamard spectroscopy.*

Microfluidics exhibit revolutionary new technological capabilities due to the precise and flexible channel design, efficient heat exchange, high mechanical stability, and economical use of reactants.[1] Microfluidic processes, such as chemical reactions, protein crystallization, cell growth, drug discovery, and health diagnostics,[2] are traditionally monitored by optical, electrochemical, and mass spectrometry methods.[3] Nuclear magnetic resonance (NMR) spectroscopy[4] is one of the most powerful analytical techniques, because it provides versatile spectroscopic, spatial, and dynamic information, and, contrary to optical methods, it allows the noninvasive, tracer-less analysis of opaque materials. The versatile analytical toolbox of NMR spectroscopy can also be exploited in microfluidic applications, if the sensitivity is boosted by using ultrasensitive miniaturized coil designs, such as microsolenoids, planar surface coils or microcoils, microstriplines, and microslots,[5] or by increasing the nuclear spin polarization degree by hyperpolarization methods, such as spin-exchange optical pumping or parahydrogen-induced polarization techniques.[6] Remote detection NMR, in which the encoding of spin coherences and the detection of signal are spatially separated,[7] allows characterizing the whole microfluidic channel network while utilizing the high sensitivity of microcoils,[8] thereby enabling time-of-flight (TOF) imaging of flow and chemical reactions of fluids in microfluidic devices.[6a–d,9]

Here we demonstrate that novel remote detection based NMR methods provide an unforeseen combination of detailed chemical and spatial information by investigating the gas phase hydrogenation reaction of propene into propane in a lab-on-a-chip reactor. The reactor consists of 36 parallel microchannels (length 1 cm, cross section $50 \times 50\ \mu m^2$) coated with platinum catalyst (see the Supporting Information). The reaction temperature was about 40 °C. The experimental setup (Figure 1 a) includes a large birdcage coil around the reactor chip that is used, along with magnetic field gradients, for encoding chemical and spatial information in the nuclear spin coherences of fluid molecules in the chip. The information is read out by an ultrasensitive microsolenoid[8] wound around the outlet capillary when the fluid flows out. The detection coil is about 800 times more sensitive than the encoding coil,[9c] and this huge sensitivity gain enables reaction imaging in spite of the extremely small channel volumes and low density of gas. The resolution of the ^1H detection coil spectrum (Figure 1 b) is high enough to distinguish the propane and propene signals, and therefore it is possible to process separate TOF images corresponding to the reagent and the reaction product (Figure 1 d and Movie S1). The images corresponding to the shortest TOF show the signal of the gas close to the chip outlet, because this gas arrives first at the detection coil, and the gas in the upper part of the reactor is detected at longer TOF. In order to get a high enough signal-to-noise ratio (SNR), 32 scans were accumulated.

The images processed using the propane (reaction product) signal show that the reaction yield is larger in the outermost channels than in the middle channels because of a slower flow velocity and a longer overall flow path in the former.[9c] By determining the position of the maximum signal amplitude as a function of time, we estimated that the flow velocity in the outermost and middle channels was about 27 and 41 $mm\,s^{-1}$, respectively. However, as described in our previous work,[9c] the images do not show the active reaction regions along the flow direction accurately, because the

[*] Dr. V.-V. Telkki, M. Sc. A. Selent
NMR Research Group, Department of Physics, University of Oulu
P.O. Box 3000, 90014 Oulu (Finland)
E-mail: ville-veikko.telkki@oulu.fi
Homepage: http://cc.oulu.fi/~nmrwww/
Dr. V. V. Zhivonitko, Prof. I. V. Koptyug
Laboratory of Magnetic Resonance Microimaging
International Tomography Center SB RAS
3A Institutskaya St., Novosibirsk 630090 (Russia)
and
Novosibirsk State University
Pirogova St. 2, Novosibirsk 630090 (Russia)
Dr. G. Scotti, M. Sc. J. Leppäniemi, Prof. S. Franssila
Department of Materials Science and Engineering, Aalto University
P.O. Box 16200, 00076 Aalto (Finland)

[**] The financial support by the grants from the Academy of Finland (no 270195), RFBR (12-03-00403-a), the Council on Grants of the President of the Russian Federation (MK-1329.2014.3), and by the Ministry of Education and Science of the Russian Federation is gratefully acknowledged. A.S. thanks the Graduate School of Computational Chemistry and Molecular Spectroscopy (LASKEMO) for funding.

Supporting information for this article is available on the WWW under http://dx.doi.org/10.1002/anie.201405681.

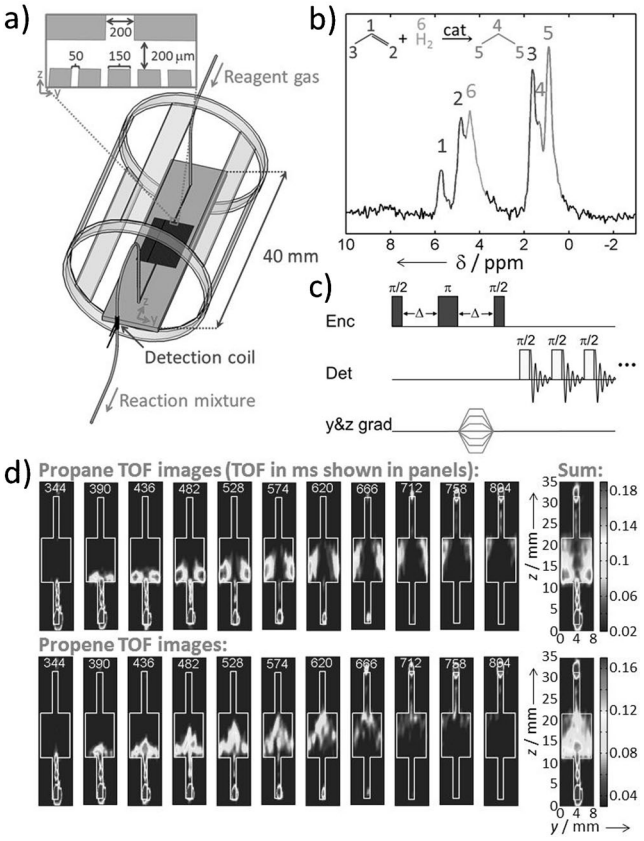

Figure 1. Remote detection NMR imaging of propene hydrogenation to propane in a lab-on-a-chip reactor. a) Experimental setup including the reactor chip (gray) as well as encoding (light gray) and detection (black) coils. b) ^{1}H NMR spectrum of the flowing gas mixture measured by the detection coil (the number of accumulated scans was 128). c) The TOF imaging pulse sequence. d) TOF flow images processed using the propane or propene methyl group signal of the detection coil spectrum. The sum of the images is shown on the right. The number of consecutive free induction decays (FIDs) collected during one scan was 40 and the time resolution (the time between the detection pulses) was 23 ms. The number of accumulated scans was 32, the resolution in the *y* and *z* directions was 0.5 and 1.75 mm, respectively, and the total experiment time was 2 h 44 min. (A colored version can be found in Figure S2.)

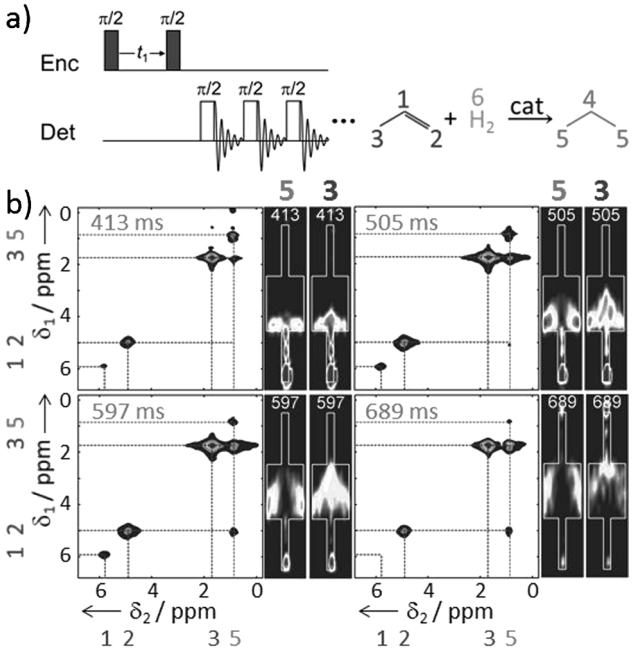

Figure 2. Remote detection exchange spectroscopy (RD-EXSY). a) The pulse sequence of RD-EXSY. b) 2D TOF EXSY spectra along with corresponding TOF images showing the position of the molecules during the signal encoding (left: propane-encoded; right: propene-encoded images). The number of complex data points was 256 in the direct and 64 in the indirect spectral dimensions. The spectral width was 40 ppm in the direct dimension and 7 ppm in the indirect dimension. The number of accumulated scans was 128 and the total experiment time was 2 h 15 min. The signals measured at four successive TOF instances were summed up to increase the SNR and consequently the effective TOF resolution in the images was 4×23 ms $=92$ ms. (A colored version can be found in Figure S3.)

spatial encoding in spin coherences is preserved in the reaction, and the propene molecules that convert to propane after the encoding also contribute to the images constructed using the detected propane signal. Consequently, even the signal from the inlet capillary is visible in the images processed using the propane signal at TOF of 666–804 ms, although there is no catalyst (and thus no propane) in the capillary. Furthermore, TOF images cannot expose reaction intermediates and whether the reaction is reversible or irreversible, because the chemical information is read out after the reactor.

Remote detection exchange spectroscopy (RD-EXSY) provides a solution to the above-mentioned issues. Its pulse sequence (Figure 2a) includes preparation and evolution periods similar to the conventional 2D EXSY,[10] but the signal is detected outside the reactor by a train of detection coil $\pi/2$ pulses. The sequence is also equivalent to the sequence used for measuring an indirect remote detection spectrum;[7] however, now it is, for the first time, used in exchange spectroscopy. Apart from correlating the chemical information in the chip with that in the detection coil, RD-EXSY includes unique TOF information that can be converted into spatial information by correlating the results with the TOF images. The diagonal signal at $\delta_1=\delta_2=0.9$ ppm (see Figure 2b and Movie S2) arises from the spins that were in the propane methyl group both during the signal encoding and detection. Its amplitude decreases with increasing TOF, and at TOF $=689$ ms, it is almost zero, because, as the TOF images in Figure 2b show, this signal arises from the molecules encoded in the upper part of the reactor, and the propane concentration in that region is very low. The cross peak at $\delta_1=1.7$ ppm and $\delta_2=0.9$ ppm, in turn, originates from the spins that were in the propene methyl group during encoding, but turned into the propane methyl group due to the hydrogenation prior to detection. The amplitude of the cross peak increases with increasing TOF, because the molecules have more time and reactor space to react after the indirect spectral encoding. The existence of the cross peak unambiguously shows that propene is converted into propane between the encoding and detection events and that the encoding of spin coherences is preserved in the reaction. Furthermore, as there is no cross peak on the other side of the

diagonal, RD-EXSY confirms that the reaction is irreversible. This kind of information is extremely valuable when investigating more complex reactions. RD-EXSY spectra may also reveal reaction intermediates with a sufficiently long lifetime on the NMR time-scale, but in this reaction no such intermediate exists. We note that Anwar et al.[11] used a related method to investigate a pH-triggered chemical transformation. They saturated a particular signal of a reagent prior to the reaction by a coil wrapped around the inlet tubing, and observed the spin coherence transformation after the reaction by another coil around the outlet tubing. By varying the saturation frequency, they were able to determine a 2D correlation map of the frequencies before and after the pH change.

Direct spatial encoding would be more accurate than the indirect conversion of TOF information into spatial information by means of TOF images; however, spatially encoded RD-EXSY would lead to far too long experiment times due to the massive number of indirect spectral and spatial encoding steps. Nevertheless, the encoding of the first, indirect spectral dimension can be implemented in a very efficient manner by using the principles of Hadamard spectroscopy,[12] in which the phases of the spectral peaks of interest are varied by means of simultaneous selective encoding according to the rows of a Hadamard matrix, and the signals are correlated with the frequencies of the second (direct) spectral dimension by applying a Hadamard transform consisting of additions and subtractions of the measured spectra. Hadamard encoding requires the number of indirect spectral phase encoding steps to be equal to the number of signals of interest, whereas the number needed in conventional 2D NMR is much larger, fundamentally defined by the ratio of the spectral width to the smallest frequency difference of adjacent signals. In addition, each Hadamard scan includes the contribution of all the spins of interest, and therefore the signal-to-noise ratio is higher than in a series of one-dimensional spectra acquired with single selective excitation. In the propene hydrogenation spectrum (Figure 1b), the smallest frequency difference between adjacent signals is about 100 Hz, while the spectral width is about 1800 Hz. Consequently, conventional indirect spectral encoding with equal SNR would result in at least 18 times longer experiments (total experiment time more than 80 h) than with Hadamard encoding. Hadamard spectroscopy has been applied, e.g., to fast protein resonance assignment, ligand screening, diffusion and relaxation measurements, single-scan 2D NMR, and hyperpolarization applications,[13] but, to the best of our knowledge, this is the first application for spectral encoding in chemical reaction imaging.

When imaging propene hydrogenation, it is enough to select only two signals for the Hadamard encoding, one from the reagent and the other from the product. We selected the most intense signals, namely propene and propane methyl group signals at 1.7 and 0.9 ppm, respectively. Consequently, the phases of the signals can be encoded according to the simplest, second order Hadamard matrix.[12] After the first encoding, both signals have the same phase, while in the second encoding the phase of the propene signal is inverted. We implemented the phase change by applying a selective π inversion pulse prior to the spatial encoding (Figure 3a).

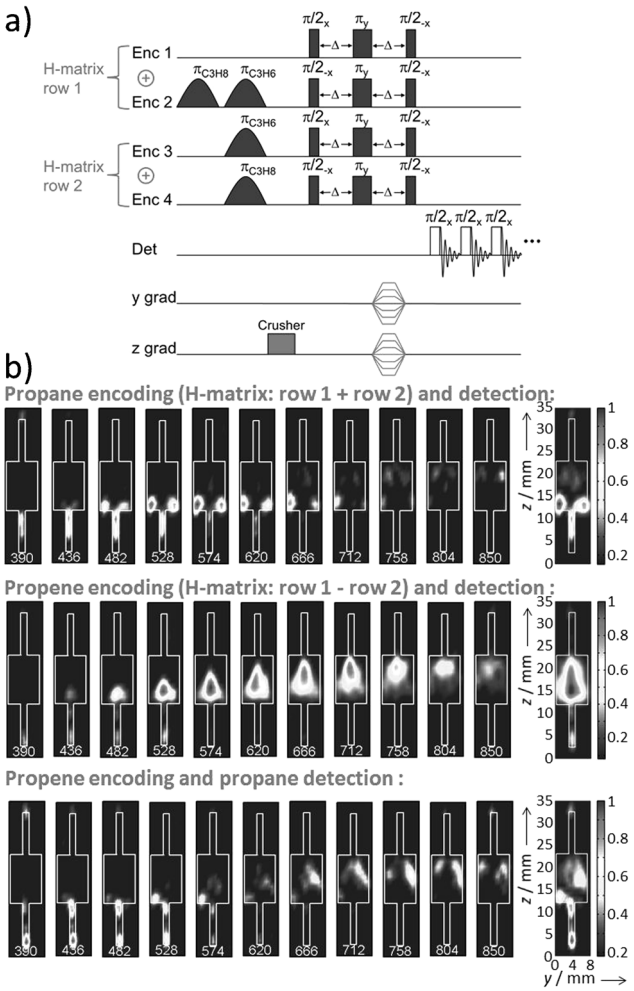

Figure 3. Hadamard-encoded TOF imaging. a) The pulse sequence of spatially resolved Hadamard-encoded RD-EXSY. b) TOF images with propane encoding and detection (top), propene encoding and detection (middle), and propene encoding and propane detection (bottom). The sum of the images is shown on the right. The number of accumulated scans was 32, the resolution in the *y* and *z* directions was 1.0 and 2.2 mm, respectively, and the total experiment time was 4 h 22 min. The signals measured at two successive TOF instances were summed up to increase the SNR and consequently the effective TOF resolution in the images was 2×23 ms = 46 ms. (A colored version can be found in Figure S4.)

Because the pulse angle was not perfectly π and because the effect of relaxation was quite significant during the relatively long inversion pulse, the inversion was not perfect. This would lead to a decreased signal amplitude of the inverted signal and consequently to artefacts in the Hadamard transform. We circumvented this problem by repeating each encoding step without the original selective π pulse, but with the selective π pulse affecting the signal untouched in the first encoding, along with the inversion of the phase of the first π/2 pulse (see Figure 3a). The results of these two measurements were then added together. This procedure ensures that all the signals have experienced similar imperfect inversion effects, enabling the Hadamard transform. The Hadamard encoding of the indirect chemical EXSY information was followed by the spatial encoding similar to TOF imaging. Altogether the

spatially resolved TOF EXSY can be considered to be a five-dimensional experiment, including two spectral, two spatial (due to the planar geometry of the reactor), and one TOF dimensions.

Hadamard-encoded TOF EXSY images processed using the propane signal both in the encoding and detection (Figure 3b and Movie S3) emphasizes lower parts of the reactor compared to the propane-detected TOF images (Figure 1d), confirming that, contrary to the TOF images, the propene converted into propane after the encoding does not contribute to these images. Hence, these images reflect more accurately the active reaction regions along the flow direction. The amplitude in the sum of the TOF images is directly proportional to the product yield, if the relaxation is insignificant. However, in this case relaxation weighting should be quite significant, because T_1 relaxation time of propane in the platinum-coated channels is close to the corresponding value of propene, which was determined to be about 270 ms.[9c] The maximum signal value is found in the lowest parts of the outermost channels, whereas the signal amplitude in the corresponding region of the propene-encoded and -detected image is almost zero, implying that the reaction yield in the end of the outermost channels is much higher than in the middle channels. This is reasonable because the overall travel time through the outermost channels is almost double that that through the middle channels due to longer path length and a lower flow velocity.

The propene-encoded and propane-detected images, in turn, highlight the upper parts of the reactor, which is reasonable, because the images originate from the propene that has not reacted before the encoding step but that is converted into propane between the encoding and detection. There is also some spurious signal arising from the outlet tubing around $z = 3$ mm due to the imperfect excitation profile of the selective pulse and the field inhomogeneity at the edges of the encoding coil. The field homogeneity and chemical resolution both in the encoding and detection regions could be improved by magnetic susceptibility matching, which may also be necessary when spectral lines of more complex substances are desired to be resolved.[8] Furthermore, both chemical and spatial resolution could be improved or, alternatively, experiment time could be shortened by implementing compressed sensing.[9b] The chemical resolution also depends on the bandwidth of the pulses used for Hadamard-encoding. We note that, contrary to the TOF imaging, spatially resolved Hadamard RD-EXSY make it possible also to produce TOF images of sufficiently long-lived reaction intermediate products, if they existed.

In summary, remote detection NMR increases the sensitivity of a lab-on-a-chip NMR experiment by several orders of magnitude, allowing even gas phase chemical reaction imaging in a lab-on-a-chip reactor in spite of the low density of gas and small channel volumes. We showed that the RD-EXSY method provides unique chemical information, revealing reaction pathways and intermediate products, and the TOF information can be converted into indirect spatial information by means of TOF images, showing the active reaction regions. Furthermore, direct spatial information can be added to RD-EXSY efficiently by implementing Hadamard encoding of the indirect spectral dimension, allowing a more accurate characterization of the active regions, while retaining other advantages of RD-EXSY. The products of microfabrication technology employed in chemistry include various microfluidic devices such as reactors, mixers, separators, heat exchangers, and analyzers.[14] Microfluidic reactors are expected to become the chemists' round-bottomed flask of the future as they provide capabilities that are hardly accessible with large-scale chemical systems.[15] The NMR methods developed here will raise the chemical analysis of lab-on-a-chip as well as other reactors to a new level.

Received: May 27, 2014
Revised: July 29, 2014
Published online: August 28, 2014

Keywords: Hadamard spectroscopy · lab-on-a-chip · microfluidics · NMR spectroscopy · reactor imaging

[1] G. M. Whitesides, *Nature* **2006**, 442, 368 – 373.
[2] a) A. J. deMello, *Nature* **2006**, *442*, 394 – 402; b) H. Song, D. L. Chen, R. F. Ismagilov, *Angew. Chem. Int. Ed.* **2006**, *45*, 7336 – 7356; *Angew. Chem.* **2006**, *118*, 7494 – 7516; c) J. El-Ali, P. K. Sorger, K. F. Jensen, *Nature* **2006**, 442, 403 – 411; d) P. S. Dittrich, A. Manz, *Nat. Rev. Drug Discovery* **2006**, *5*, 210 – 218; e) P. Yager, T. Edwards, E. Fu, K. Helton, K. Nelson, M. R. Tam, B. H. Weigl, *Nature* **2006**, *442*, 412 – 418.
[3] J. Wu, M. Gu, *J. Biomed. Opt.* **2011**, *16*, 080901.
[4] B. Blümich, *NMR Imaging of Materials*, Oxford University Press, Oxford, **2000**.
[5] a) E. Harel, *Lab Chip* **2009**, *9*, 17 – 23; b) J. D. Trumbull, I. K. Glasgow, D. J. Beebe, R. L. Magin, *IEEE Trans. Biomed. Eng.* **2000**, *47*, 3 – 7; c) H. Wensink, F. Benito-Lopez, D. C. Hermes, W. Verboom, H. J. G. E. Gardeniers, D. N. Reinhoudt, A. van den Berg, *Lab Chip* **2005**, *5*, 280 – 284; d) S. Ahola, F. Casanova, J. Perlo, K. Münnemann, B. Blümich, S. Stapf, *Lab Chip* **2005**, *6*, 90 – 95; e) S. Ahola, V.-V. Telkki, S. Stapf, *Lab Chip* **2012**, *12*, 1823 – 1830; f) J. Bart et al., *J. Am. Chem. Soc.* **2009**, *131*, 5014 – 5015; g) H. Krojanski, J. Lambert, Y. Gerikalan, D. Suter, R. Hergenröder, *Anal. Chem.* **2008**, *80*, 8668 – 8672.
[6] a) C. Hilty, E. E. McDonnell, J. Granwehr, K. L. Pierce, S. Han, A. Pines, *Proc. Natl. Acad. Sci. USA* **2005**, *102*, 14960 – 14963; b) V.-V. Telkki, C. Hilty, S. Garcia, E. Harel, A. Pines, *J. Phys. Chem. B* **2007**, *111*, 13929 – 13936; c) V.-V. Telkki, V. V. Zhivonitko, S. Ahola, K. V. Kovtunov, J. Jokisaari, I. V. Koptyug, *Angew. Chem. Int. Ed.* **2010**, *49*, 8363 – 8366; *Angew. Chem.* **2010**, *122*, 8541 – 8544; d) V. V. Zhivonitko, V.-V. Telkki, I. V. Koptyug, *Angew. Chem. Int. Ed.* **2012**, *51*, 8054; *Angew. Chem.* **2012**, *124*, 8178; e) L.-S. Bouchard, S. R. Burt, M. S. Anwar, K. V. Kovtunov, I. V. Koptyug, A. Pines, *Science* **2008**, *319*, 442 – 445.
[7] A. J. Moule, M. Spence, S. Han, J. Seeley, K. Pierce, S. Saxena, A. Pines, *Proc. Natl. Acad. Sci. USA* **2003**, *100*, 9122 – 9127.
[8] D. L. Olson, T. L. Peck, A. G. Webb, R. L. Magin, J. V. Sweeder, *Science* **1995**, *270*, 1967 – 1970.
[9] a) E. Harel, C. Hilty, K. Koen, E. E. McDonnell, A. Pines, *Phys. Rev. Lett.* **2007**, *98*, 017601; b) V. S. Bajaj, J. Paulsen, E. Harel, A. Pines, *Science* **2010**, *330*, 1078 – 1081; c) V. V. Zhivonitko, V.-V. Telkki, J. Leppäniemi, G. Scotti, S. Franssila, I. V. Koptyug, *Lab Chip* **2013**, *13*, 1554 – 1561.
[10] J. Jeener, B. H. Meier, P. Bachmann, R. R. Ernst, *J. Chem. Phys.* **1979**, *71*, 4546 – 4553.
[11] M. S. Anwar, C. Hilty, C. Chu, L.-S. Bouchard, K. L. Pierce, A. Pines, *Anal. Chem.* **2007**, *79*, 2806 – 2811.

[12] E. Kupče, T. Nishida, R. Freeman, *Prog. Nucl. Magn. Reson. Spectrosc.* **2003**, *42*, 95 – 122.
[13] a) E. Lescop, R. Rasia, B. Brutscher, *J. Am. Chem. Soc.* **2008**, *130*, 5014 – 5015; b) M. Feliz, J. García, E. Aragón, M. Pons, *J. Am. Chem. Soc.* **2006**, *128*, 7146 – 7147; c) C. A. Steinbeck, B. F. Chmelka, *J. Am. Chem. Soc.* **2005**, *127*, 11624 – 11635; d) A. Tal, B. Shapira, L. Frydman, *Angew. Chem. Int. Ed.* **2009**, *48*, 2732 – 2736; *Angew. Chem.* **2009**, *121*, 2770 – 2774; H.-Y. Chen, C. Hilty, *Anal. Chem.* **2013**, *85*, 7385 – 7390.
[14] a) *Sustainable industrial processes* (Eds.: F. Cavani, G. Centi, S. Perathoner, F. Trifirò), Wiley-VCH, Weinheim, **2009**, p. 599; b) K. F. Jensen, *Chem. Eng. Sci.* **2001**, *56*, 293 – 303.
[15] K. Geyer, J. D. C. Codee, P. H. Seeberger, *Chem. Eur. J.* **2006**, *12*, 8434 – 8442.

